

# Improving outcomes in intracerebral hemorrhage through microglia/macrophage-targeted IL-10 delivery with phosphatidylserine liposomes

Ranran Han<sup>a,1</sup>, Xi Lan<sup>a,1</sup>, Zheng Han<sup>b,c,d,1</sup>, Honglei Ren<sup>a</sup>, Safiya Aafreen<sup>b,e</sup>,  
Wenshen Wang<sup>b,c</sup>, Zhipeng Hou<sup>b</sup>, Tianyue Zhu<sup>a,e</sup>, Andrew Qian<sup>a,e</sup>, Xiaoning Han<sup>a,\*\*</sup>,  
Raymond C. Koehler<sup>a,\*\*\*</sup>, Guanshu Liu<sup>b,c,\*</sup>

<sup>a</sup> Department of Anesthesiology and Critical Care Medicine, The Johns Hopkins University School of Medicine, Baltimore, MD, 21205, USA

<sup>b</sup> Russell H. Morgan Department of Radiology, Johns Hopkins University School of Medicine, Baltimore, MD, USA

<sup>c</sup> F.M. Kirby Research Center, Kennedy Krieger Institute, Baltimore, MD, USA

<sup>d</sup> Center for Health Systems Innovation, Oklahoma State University, Stillwater, OK, 74078, USA

<sup>e</sup> Department of Biomedical Engineering, Johns Hopkins University, Baltimore, MD, USA

## ARTICLE INFO

### Keywords:

Intracerebral hemorrhage (ICH)  
Liposomes  
Phosphatidylserine–liposomes (PSL)  
IL-10  
Microglia and macrophage-targeted drug  
delivery

## ABSTRACT

Intracerebral hemorrhage (ICH) remains the most lethal type of stroke, and effective clinical therapies that can speed up hematoma resolution after ICH are still lacking. While the beneficial effects of IL-10 on ICH recovery have been demonstrated, the clinical translation of IL-10 requires effective delivery methods by which sufficient IL-10 can be delivered to ICH-affected regions in the brain. Here we report the use of a phosphatidylserine (PS) liposome (PSL)-based nanoparticle system for microglia/macrophage-targeted delivery of IL-10 in ICH. We first prepared IL-10-conjugated PSL (PSL-IL10) and characterized their immunomodulating effects in vitro. Then we evaluated the therapeutic effects, including hematoma absorption, short-term outcomes, and neuroinflammation, of intranasally administered PSL-IL10 (3 µg IL-10 per mouse, 2 h post-ICH) in a collagenase-induced ICH mouse model. We also isolated microglia/macrophages from the mouse brains with ICH to analyze their morphology, phagocytosis ability, and polarization. Our study reveals that, 1) PSL-IL10 treatment resulted in significantly improved outcomes and accelerated hematoma resolution in the acute phase of ICH; 2) PSL-IL10 inhibited glial activation and down-regulated pro-inflammatory cytokine production; 3) PSL-IL10 induced Iba1<sup>+</sup> cells with a stronger phagocytosis ability; 4) PSL-IL10 activated STAT3 and upregulated CD36 expression in microglia/macrophage. These findings collectively show that PSL-IL10 is a promising nanotherapeutic for effectively ameliorating ICH.

## 1. Introduction

Intracerebral hemorrhage (ICH) is the second most common cause of stroke following ischemic stroke, accounting for 27.9% of all new strokes in 2019 globally [1]. Among all strokes, ICH has the highest mortality rate, with early-term mortality of about 30%–40%, and the highest disability rate, with approximately 70% of patients experiencing

long-term deficits [2,3]. ICH causes brain injury first by hematoma formation, and expansion ensues from initial bleeding, causing mechanical damage (mass effect) to surrounding brain tissue. After the primary injury, secondary injury follows due to perihemorrhagic inflammation, toxic products of blood breakdown, and perihematomal edema, continuing to cause brain injury and neuronal death [4,5]. Despite tremendous effort devoted to developing treatments aiming to

\* Corresponding author. Russell H. Morgan Department of Radiology, Johns Hopkins University School of Medicine, Baltimore, 707 N Broadway, Baltimore, MD, 21205, USA.

\*\* Corresponding author. Department of Anesthesiology and Critical Care Medicine, The Johns Hopkins University School of Medicine, 720 Rutland Ave, Ross 370, Baltimore, MD 21205, USA

\*\*\* Corresponding author. Department of Anesthesiology and Critical Care Medicine, The Johns Hopkins University School of Medicine, 720 Rutland Ave Traylor 809, Baltimore, MD 21205.

E-mail addresses: [xhan15@jhmi.edu](mailto:xhan15@jhmi.edu) (X. Han), [rkoehler@jhmi.edu](mailto:rkoehler@jhmi.edu) (R.C. Koehler), [gaunshu@mri.jhu.edu](mailto:gaunshu@mri.jhu.edu) (G. Liu).

<sup>1</sup> These authors contributed equally to this work.

reduce hematoma volume and thereby limit both primary and secondary brain injury after ICH, there is no effective clinically available treatment yet [6]. Surgical treatments, including hematoma evacuation [7–9] and thrombolytic irrigation [10] have failed in clinical trials thus far. New medicinal treatments that can effectively limit hematoma expansion and accelerate hematoma resolution are desperately needed.

The endogenous hematoma clearance system is activated after ICH, mainly through the phagocytosis by microglia/macrophages (M/MΦs). Within 1 h after ICH, microglia are activated in response to hematoma [11]. Monocytes in circulation are recruited and mature into macrophages in the brain several hours after ICH [12,13]. While the exact role of the pro-inflammatory phenotype of M/MΦs is still debated [14], it is believed that the adaptive regulatory phenotypes of M/MΦs are beneficial to hematoma resolution and neuroprotection, prominently attributed to their effects to clear erythrocytes and phagocytose cell debris [3,15,16]. Hence, identifying and optimizing therapeutics that can convert the phenotype of M/MΦs from pro-inflammatory to regulatory phenotype has been of great interest. For example, Xu et al. recently confirmed the effectiveness of interleukin-4 in facilitating hematoma resolution and functional recovery after ICH [17]. We and others revealed that another classic anti-inflammatory cytokine, interleukin-10 (IL-10), can exert substantial neuroprotection in ICH by eliciting M/MΦ phagocytosis function and anti-inflammatory polarization [13,18–21]. In the central nervous system (CNS), IL-10 is primarily produced by microglia [22,23]. Our previous study confirmed that microglia-derived IL-10 accelerated post-ICH hematoma clearance through the signal transducer and activator of transcription 3 (STAT3)-dependent pathway [18,24]. However, the use of IL-10 as an effective therapy requires suitable drug delivery methods by which sufficient IL-10 can be delivered to the perihematomal regions because directly administering IL-10 for treating CNS disorders has limited translation potential [25]. Based on the past failures in the clinical trials of using recombinant human IL-10 (rhIL-10) to treat inflammatory bowel disease [26,27], pancreatitis [28], endotoxemia [29], and rheumatoid arthritis [30], systemic administration of free IL-10 faces many challenges including low efficiency of targeted delivery due to short half-life [31,32] and unwanted effects on other immune cells, including T and B cells, dendritic cells, mast cells, and neutrophils [33]. Therefore, new effective M/MΦs-targeted delivery methods are needed to translate IL-10-based ICH treatment to clinical use.

This study aimed to develop a new nanoparticle-based approach to accomplish efficient, targeted delivery of IL-10 to M/MΦs in the brain after ICH. We chose phosphatidylserine (PS)-presenting liposomes (PSLs) as the drug carrier because of its well-documented M/MΦs targeting ability. PS is a type of negatively charged membrane phospholipid mainly distributed in the inner leaflet of the plasma membrane and endocytic membranes of normal cells. The externalization of PS is a hallmark of cell apoptosis and necroptosis [34], and PS presentation is one of the most prominent “eat-me” signals to make apoptotic cells recognized by phagocytes [35,36]. Mounting studies have exploited the “eat-me” feature of PS to construct PS-presenting liposomes (PSLs) to target macrophages specifically [37–40]. While PSLs can promote the transformation of macrophages from pro-inflammatory to regulatory phenotype [41–44], the effect is only moderate, and many studies just used PSLs as macrophage-targeted drug carriers to deliver anti-inflammatory therapeutics [42,45]. For instance, Toita et al. recently reported the substantially enhanced anti-inflammatory and anti-obesity effects of IL-10 conjugated PSLs compared to direct administration of IL-10 [46]. They attributed the enhancement of anti-inflammatory effects to the synergized stimulation of both PS and IL-10 receptor-mediated signaling pathways by PSL-IL10. Inspired by these previous studies, we rationalized that PSLs can be used as an effective M/MΦs-targeted delivery vehicle to improve the delivery and treatment efficacy of IL-10 against brain injury after ICH. In this study, we focused on evaluating the feasibility of intranasally administered PSL-IL-10 for treating ICH in an experimental animal model and

illustrating the mechanism. To the best of our knowledge, this is the first report on the M/MΦs-targeted, nanoparticle-mediated IL-10 ICH treatment. The results of this study will provide insights into future translational research of cytokine-based immunotherapy for effectively combatting ICH.

## 2. Methods and material

### 2.1. Preparation and characterization of PSL-IL10

Unless otherwise noted, all chemicals were purchased from Sigma Aldrich (Saint Louis, MO, USA). Brain phosphatidylserine (PS), egg phosphatidylcholine (PC), and rhodamine-B- phosphatidylethanolamine (PE) were purchased from Avanti Polar Lipids, Inc.

The synthesis of PSL-IL10 is illustrated in Fig. 1. In brief, 150 μL recombinant murine IL-10 (PeproTech, Cat# 210-10, 60 μg/mL) was incubated with 10 μL palmitic acid-NHS (Sigma-Aldrich Cat# P1162, 20 mg/mL in ethanol) at 37 °C overnight under magnetic stirring according to a previously published procedure [46]. The product was purified by G50 sepharodex beads to remove unconjugated IL-10 and concentrated using an Amicon Ultra-0.5 centrifugal filter (3000 kDa MWCO) for 4 min at 3000 rpm.

Phosphatidylserine-Liposomes (PSLs) were prepared using the lipid film hydration method as described previously [47–49]. In brief, brain PS (0.32 mL, 25 mg/mL) and egg PC (0.275 mL, 25 mg/mL) at a molar ratio of 5.4:4.6, were dissolved in chloroform, with 0.5% rhodamine-B-PE being added to enable fluorescence imaging of PSLs. A 54% of PS was chosen to obtain a strong binding affinity to the cell surface PS-receptor, T-cell immunoglobulin mucin protein 4 (Tim4) as shown in the study by Hirose et al. [50]. The lipid mixture was dried in a glass tube for 20 min under a gentle stream of air, followed by freeze-drying for 30 min, and resuspended in 0.5 mL phosphate-buffered saline (PBS). The solution was homogenized at 60 °C for 1.5 h, being shaken every 30 min, and then passed sequential extrusion through 0.4, 0.2, and 0.1 μm polycarbonate membranes using an Avanti Mini-Extruder, with at least 20 passages performed.

To 200 μL PSL solution, 150 μL of the synthesized IL10-palmitic acid (~60 μg/mL) was added, and the mixture was incubated for 30 min at room temperature. The size of the resulting PSL-IL10 was characterized by dynamic light scattering (DLS) using a Nanosizer ZS90 (Malvern Instruments, Southborough, MA) and transmission electron microscopy using a Zeiss Libra 120 TEM operated at 120 KV and equipped with an Olympus Veleta camera (Olympus Soft Imaging Solutions GmbH, Münster, Germany). The amount of IL10-palmitic acid incorporated into PSLs was assessed using a Micro BCA™ Protein Assay Kit (Thermo Fisher Scientific) according to the manufacturer’s instructions. After the absorbance of each sample at 562 nm (OD<sub>562</sub>) was measured using a NanoDrop™ spectrophotometer (Thermo Fisher Scientific), the loading efficiency of IL10 was calculated as: Loading rate (%) = (OD<sub>562</sub>, PSL-IL10 - OD<sub>562</sub>, PSL)/OD<sub>562</sub>, IL10-palmitic acid × 100%.

### 2.2. In vitro effects of PSL-IL10 on microglia

#### 2.2.1. Primary microglia cell culture

The mouse pups at postnatal day 0–1 from Cx3cr1<sup>GFP/+</sup> mice (Jackson Lab) were decapitated rapidly. The brain was removed and dissociated into single cells with papain as described previously [51]. The primary glial cells were cultured with DMEM/F12 (#11330057, Thermo Fisher Scientific) with 10% fetal bovine serum (FBS) (#10438026, Thermo Fisher Scientific). At 14 days of culture in vitro, the primary glial cells were shaken at 200 rpm at 37 °C for 4 h and the primary microglia were collected from the supernatant. To address whether microglia engulf PSL-IL10, the primary cultured microglia were cultured in cell culture slide chamber (Thermo Scientific) at 10<sup>4</sup> cells per well for 3 days and incubated with rhodamine B-labeled PSL-IL10 (3.2 × 10<sup>8</sup> particles/mL) for 24 h. The primary microglia were washed with

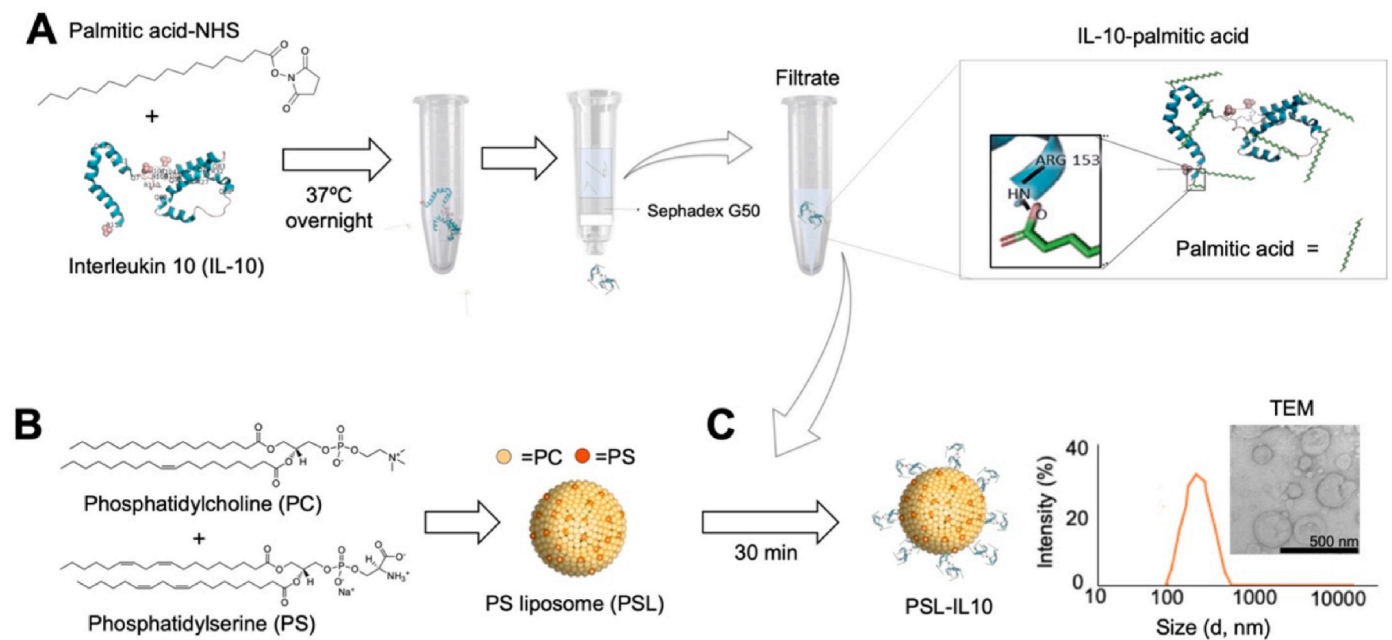


**Fig. 1.** Schematic illustration of the synthesis of PSL-IL10. **A)** Synthesis of IL10-palmitic acid. **B)** Synthesis of PSL, and **C)** Synthesis of PSL-IL10, with the right panel showing their size characteristics studied by dynamic light scattering (DLS) and transmission electron microscopy (TEM).

phosphate-buffered saline (PBS), then fixed with 4% paraformaldehyde (PFA). The images were taken with Nikon E90i microscope.

### 2.2.2. Phagocytosis assay

Primary cultured microglia were incubated with PSL-IL10 for 24 h, then treated with pH-sensitive pHrodo® Red Zymosan Bioparticles (P35364, Thermo Fisher Scientific) according to the manufacturer's instructions. Due to the pH-sensitive nature of the fluorescence dye, the beads are only fluorescent (ex/em = 560/585 nm) in endosomes following phagocytosis. Three hours later, cells were washed with PBS and fixed with 4% PFA. The images were taken with Leica microscope (DM6 FL, USA). The phagocytosis ability of cells was quantified by fluorescent intensities.

### 2.3. Animals

All animal protocols were conducted in compliance with the ARRIVE and RIGOR guidelines for the use of experimental animals [52], and approved by the Institutional Animal Care and Use Committee at Johns Hopkins University School of Medicine. Wild-type C57BL/6J mice (male, 2-month-old) and Cx3cr1<sup>GFP/+</sup> mice were purchased from Jackson Laboratory (Bar Harbor, ME). CD36<sup>flox/flox</sup> mice and LysM<sup>Cre</sup> ± CD36<sup>flox/flox</sup> mice were obtained from Dr. Ira J. Goldberg (New York University, New York, NY).

### 2.4. ICH model

Under anesthetization using 1%–3% isoflurane inhalation and ventilation with oxygen-enriched air (20% O<sub>2</sub>:80% air) by a nose cone, mice received an intracranial injection of 0.5 μL of collagenase VII-S (#C2399, MilliporeSigma, St. Louis, MO, USA) at 0.15 U/μL (0.1 μL per minute) in the left striatum (0.6 mm anterior and 2.0 mm lateral to the bregma, and 3.0 mm in depth). During the operation, body temperature of the mice was maintained at 37.0 ± 0.5 °C. Sham-operated mice received a saline injection at the same location and injection volume. All animals were included in the final analysis, except those who died or had a >23 out of 24 score on the neurologic deficit assessment within 24 h of surgery. The 24-point neurologic deficit score was calculated by summing the scores of six neurologic tests: body

symmetry, gait, climbing, circling behavior, front limb symmetry, and compulsory circling, with a score of severity being graded between 0 and 4 according to the deficit scoring system described by Clark et al. [53].

### 2.5. Treatment

Animals were randomly assigned to five groups: 1) PSL-IL10, 2) PSL, 3) IL-10, 4) saline control, and 5) sham control. Each mouse received intranasal treatments of 5 μL solution containing 0.3 μg IL-10 equivalent of PSL-IL10, equivalent PSL, or 0.3 μg of IL-10, or saline, respectively. The first treatment was administered within 2 h post-ICH and subsequently once daily for 7 days. To test the dose-dependency of PSL-IL10, two additional groups of mice received PSL-IL10 at 0.03 μg or 0.1 μg IL-10 equivalent per mouse using the same treatment regimen. MRI and behavior tests were conducted for up to 28 days. At the desired time points, selected mice were euthanized and perfused with cold PBS, and with or without 4% paraformaldehyde, followed by morphological and immunohistochemical assessments, or protein analysis as detailed below.

### 2.6. Lesion volume and hematoma size analysis

Three days after ICH, brain lesion volume was evaluated by staining 25-μm-thick brain sections with Luxol fast blue (FB) and cresyl violet (CV) as described before [54]. The hematoma size at 1, 3, or 7 days after ICH was measured by scanning the freshly cut hemorrhagic brain sections (mouse brain matrix, thickness = 1 mm) according to our previously published procedures [55].

### 2.7. Brain water content

As a surrogate biomarker for brain edema, the brain water content was measured using a wet-dry weight method. At 3 days after ICH, mice were euthanized by deep anesthesia. The brains were removed and divided into ipsilateral or contralateral cortex, striatum, and cerebellum to obtain the wet weight. Then, the dry weight was collected after drying tissues at 100 °C for 24 h. The brain water content was calculated as [(wet weight-dry weight)/wet weight] × 100%.

## 2.8. Magnetic resonance imaging (MRI)

A horizontal 11.7 T MR scanner (Bruker Biospin, Billerica, MA, USA) equipped with triple-axis gradient (maximum gradient strength = 74 Gauss/cm) using a volume excitation coil and a 4-channel phased array mouse head receive-only coil was applied to perform *in vivo* MRI experiments according to previously reported procedures [56]. Briefly, multi-slice T2-weighted (T2w) images were achieved by using a rapid acquisition with relaxation enhancement (RARE) sequence with the following parameters: TR (repetition time)/TE (echo time) = 3800/60 ms, RARE-factor = 8, number of averages = 4, field of view = 15 mm × 15 mm, 28 slices with 0.5 mm slice thickness, in-plane resolution of 0.08 × 0.08 mm<sup>2</sup>, and the total acquisition time = 12 min. We manually defined the hematoma volume on days 3, 7, and 14, residual lesion volume on days 3, 7, 14 and 28, and volume of the contralateral hemisphere in the T2w images using Amira 5.4.0.

## 2.9. Neurologic deficit behavior tests

At each time point, mice were graded using a 24-point neurologic deficit scoring system and wire hanging test as described before [57].

## 2.10. Immunostaining

Brain tissues in 25- $\mu$ m-thick coronal sections were processed and stained according to our previously published protocols [58]. Different antibodies were applied, including anti-gial fibrillary acidic protein (GFAP, 1:500, #13-0300, Life Technologies), anti-CD36 (1:100, #MA5-14112, Invitrogen), anti-CD68 (1:200, #MCA1957, Bio-Rad Laboratories, Hercules, CA, USA) and anti-ionized calcium binding adaptor molecule 1 (Iba1) antibody (1:500, #019-19741, Wako, Osaka, Japan) and incubated overnight at 4 °C. After appropriate secondary antibody incubation, the nuclei were labeled by DAPI (H-1200, Vector Laboratories, Burlingame, CA, USA). Sections were examined with fluorescence microscopes (Leica DM6, FL, USA or EVOS FL auto imaging, Thermo Fisher Scientific, Frederick, MD) or a confocal microscope (Leica SP8).

## 2.11. ELISA

Pro-inflammatory cytokine concentrations in brain tissues were detected with IL-1 $\beta$  and IL-6 ELISA kits (R&D System, Minneapolis, MN, USA). The concentration was determined by comparing its absorbance at 450 nm with that of a known standard curve. The cytokine expression levels were expressed as fold change to the sham group.

## 2.12. Microglia/macrophage morphology analysis

The morphology of perihematomal Iba1-positive cells at 3 days post-ICH was analyzed with NeuroLucida software (MBF Bioscience, Williston, VT, USA) as previously described [59]. Three fields per section with a magnification of 200 × (~120 cells with intact processes) in each image were included for analysis. Cell soma size, dendrite number, and length, number of nodes and ends of Iba1<sup>+</sup> cells, and the complexity of the cells were quantified.

## 2.13. Magnetic-activated cell sorting (MACS)

On day 1 after ICH, we collected a 4 mm-thick section of the ipsilateral brain hemisphere from each randomly selected mouse in cold Hanks' buffered salt solution (HBSS; without Ca<sup>2+</sup>/Mg<sup>2+</sup>). Tissue dissociation was conducted using the GentleMACS™ Dissociator and Neural Tissue Dissociation kit (P) (#130-092-628, Miltenyi Biotec, Bergisch Gladbach, Germany) [60]. The single cell suspension was harvested after the myelin was removed using myelin removal beads (#130-096-731, Miltenyi Biotec), and M/M $\Phi$ s were magnetically separated with CD11b MicroBeads (#130-049-601, Miltenyi Biotec) and LS

columns according to the manufacturer's protocol. The sorted cells were then applied for *ex vivo* phagocytosis assay or mRNA extraction.

## 2.14. Real-time polymerase chain reaction (PCR)

We extracted total mRNA from the sorted CD11b<sup>+</sup> cell pellets and measured the mRNA concentration on a NanoDrop 2000 spectrophotometer. Then, the reverse transcription reaction was carried out with a cDNA synthesis kit (#11754250, Thermo Fisher Scientific). Real-time PCR was carried out with the TaqMan Universal Master Mix (#4440038, Thermo Fisher Scientific) and the following primers: IL1 $\beta$  (Mm00434228\_m1), IL6 (Mm00446190\_m1), IL4 (Mm00445259\_m1), Arg1 (Mm00475988\_m1), and GPADH (Mm99999915\_g1). The relative gene expression was expressed as folds of change ( $\Delta\Delta$ Ct) and normalized to that of the sham group [57].

## 2.15. Ex vivo M/M $\Phi$ phagocytosis assay

The sorted CD11b<sup>+</sup> cells were seeded on a poly-L-lysine-coated 96-well plate at 10<sup>4</sup> cells per well and cultured in DMEM/F-12 (#11330057, Thermo Fisher Scientific) with 10% FBS (#10438026, Thermo Fisher Scientific), 20 ng/ $\mu$ L M-CSF (#315-02, PeproTech, Rocky Hill, NJ) and 100 U/mL penicillin-streptomycin for 16 h. The cells were incubated with pH-sensitive pHrodo® Red Zymosan Bioparticles (P35364, Thermo Fisher Scientific) for 3 h. Then, the cells were washed with PBS and fixed with 4% paraformaldehyde, followed by immunostaining with Iba1 primary antibody and Alexa Fluor 488 conjugated secondary antibody. The images were taken with EVOS FL auto imaging (Thermo Fisher Scientific, Frederick, MD).

## 2.16. Western blot

Samples with an equal amount of total protein were loaded into and separated by 4–20% SDS-PAGE gel electrophoresis and transferred onto PVDF membrane. After blocking, the antibodies to the following proteins were applied for membrane incubation overnight: IL-10 (1:1000, ab9969, Abcam, Cambridge, UK), STAT3 (1:1000, #4904, Cell Signaling Technology, Danvers, MA, USA), phosphor-STAT3 (1:1000, #9145, Cell Signaling Technology), CD36 (1:1000, #MA5-14112, Invitrogen, Carlsbad, CA, USA),  $\beta$ -actin (1:2000, sc-47778, Santa Cruz Biotechnology, Dallas, TX, USA). Then after incubation with appropriate horseradish peroxidase-conjugated secondary antibodies, the membranes were immersed in enhanced chemiluminescence solution to detect bands under an ImageQuant ECL imager (GE Healthcare, Chicago, IL, USA) or iBright™ CL1000 imaging system (ThermoFisher Scientific). Bands were further analyzed by ImageJ software. All data were normalized to the corresponding loading control and expressed as fold change to the sham group.

## 2.17. Statistics

Data are presented as means  $\pm$  SD. Differences among multiple groups were analyzed by one-way ANOVA with an appropriate post hoc test. A two-way ANOVA or mixed-effects model with an appropriate post hoc test was applied to analyze the effects of multiple factors. Differences between two groups were analyzed using the Student's *t*-test or Mann-Whitney *U* test. All analysis was carried out with GraphPad prism 8 software. Differences with *p* values < 0.05 were considered to be significant.

## 3. Results

### 3.1. Characterization of PSL-IL10

We synthesized PSL-IL10 according to the protocol illustrated in Fig. 1. The average size of PSL-IL10 was measured to be 153.1  $\pm$  50.21

nm (diameter) by DLS (Fig. 1C and Supplementary Figs. S1A–B) and  $139.8 \pm 42.4$  nm by TEM (Fig. 1C and Supplementary Fig. S2), which was significantly larger than PSL ( $116.7$  nm  $\pm$   $5.8$  by DLS). Moreover, the polydispersity index (PDI) of PSL-IL10 (PDI = 0.203) was almost twice the value of PSL (0.112), indicating a much larger size distribution after the IL-10-palmitic acid insertion (Supplementary Fig. S1C). The zeta potentials for PSL and PSL-IL10 were  $-25.4 \pm 0.13$  mv and  $-22.7 \pm 0.20$  mv, respectively (Supplementary Fig. S1D). The loading rate of IL-10 in the final PSL-IL10 particles was determined to be 88% by the  $\mu$ BCA method.

As shown in Supplementary Fig. S3, PSL-IL10 resulted in significantly decreased expression levels of proinflammatory markers (IL-1 $\beta$ , TNF- $\alpha$ , and iNOS) and increased expression levels of anti-inflammatory markers (Arg-1, IL-10, and TGF- $\beta$ ) in LPS/IFN- $\gamma$  treated murine RAW264.7 macrophage cells. The anti-inflammatory effects of PSL-IL10 were similar to that of IL-10 but much stronger than PSL alone, indicating the effects are largely attributed to the intracellular delivery of IL-10. Importantly, treating cultured primary microglia with PSL-IL10 could significantly increase phagocytosis activity (Fig. 2).

### 3.2. Selective uptake of intranasally administered PSL-IL10 by M/M $\Phi$ s after ICH

We then evaluated the uptake and selectivity of PSL-IL10 in M/M $\Phi$ s both in vitro and ex vivo. The results show that PSL-IL10 was substantially engulfed by not only the cultured primary microglia (Supplementary Fig. S4A) but also the microglia in organotypic hippocampal slice culture (OHSC) from Cx3cr1<sup>GFP/+</sup> transgenic mice (Supplementary Fig. S4B). After confirming the desired immunomodulation effects and specific uptake in M/M $\Phi$ s in vitro experiments, we used PSL-IL10 to treat ICH mice via intranasal administration. Immunofluorescence imaging (Fig. 3A and Supplementary Fig. S5A) shows that there was a markedly increased number of activated M/M $\Phi$ s (Iba1<sup>+</sup>, green) in the peri-hematoma regions over time. More PSL-IL10 (labeled with rhodamine B, red) become visible in these regions after 24 h, with a noticeable amount of PSL-IL10 being engulfed by M/M $\Phi$ s (yellow dots pointed by white arrows). Interestingly, activated M/M $\Phi$ , along with engulfed PSLs, were observed in the contralateral hemisphere while being much less than in both peri-hematoma and hematoma core regions at 72 h after ICH. Notably, fewer PSLs were colocalized with neurons, astrocytes and vascular endothelial cells than those with Iba1<sup>+</sup> M/M $\Phi$ s (Supplementary Fig. S5). Furthermore, Western blot results showed that PSL-IL10 administration led to a significantly upregulated IL-10 brain tissue level, i.e., 3 and 1.5 folds higher - than in vehicle control tissue at days 1 and 3 after ICH, respectively (Fig. 3B).

### 3.3. PSL-IL10 ameliorated short-term outcomes after ICH

The short-term effects of PSL-IL10 on the ICH outcomes were evaluated by the lesion volumes measured by Luxol fast blue (FB)/cresyl violet (CV) staining at day 3 and T2-weighted (T2wt) MRI at 3, 7, 14 and 28 days after ICH. The staining results showed that PSL-containing 0.03,

0.1 and 0.3  $\mu$ g IL-10 produced a dose-dependent decrease in ICH lesion volume at day 3 post-ICH (Fig. 4A). The substantially reduced lesion volume at day 3 in the mice administered with PSL-IL10 (0.3  $\mu$ g) was further confirmed by T2wt MRI (Fig. 4B). The longitudinal T2wt MRI also showed that PSL-IL10 (0.3  $\mu$ g) resulted in an accelerated reduction in hematoma volume (hypointense region) after ICH compared with the vehicle group (Fig. 4B). Moreover, at the dose of 0.3  $\mu$ g, the injury volume of mice treated solely with native IL-10 was greater compared with PSL-IL10-treated mice (Supplementary Fig. S6), indicating a stronger protection exerted by PSL-IL10.

Consequently, we assessed the effects of PSL-IL10 on reducing brain edema by measuring brain water content and diffusion-weighted imaging (DWI) at 3 days after ICH. As shown in Fig. 4C, PSL-IL10 (0.3  $\mu$ g) treatment significantly suppressed the water content in the ipsilateral cortex and striatum more than that by saline and PSL. Likewise, DWI results also revealed significantly reduced edema volume in the peri-hematoma regions, where edema was shown as hyperintensity (arrows) around hemorrhagic regions (dark hole) on the ADC maps shown in Fig. 4D.

Based on the results of the above dose-dependent studies, we chose 0.3  $\mu$ g IL-10 as an effective dose which was then used in our later behavior study. We performed both the 24-point neurologic deficit score assessment and wire hanging test to evaluate the mouse motor function on days 1, 3, and 7 after ICH. Treating with PSL-IL10 significantly decreased neurologic deficit score (Fig. 4E) and prolonged falling latency in wire hanging tests on day 1 and day 3 after ICH (Fig. 4F), suggesting that PSL-IL10 accelerates the recovery of motor function. In addition, PSL-IL10 could effectively prevent the loss of body weight in the early phase after ICH (Fig. 4G). All these data demonstrate that PSL-IL10 is an effective treatment for mitigating the short-term outcomes of ICH.

### 3.4. PSL-IL10 promoted hematoma resolution after ICH

We then examined the hematoma resolution on days 1, 3, and 7 after ICH by assessing a series of 1-mm depth coronal brain slices. The hematoma size in the PSL-IL10 treated mice were significantly smaller than the vehicle group on days 3 and 7 after ICH (Fig. 5A), which was in agreement with the hematoma size results achieved by T2w MRI (Fig. 4B).

### 3.5. In vivo immunomodulation effects of PSL-IL10

We assessed the effect of PSL-IL10 on the glial activation using immunostaining. The activation of astrocytes shows increased expression of GFAP and reactive M/M $\Phi$ s express upregulation of CD68 (myeloid cell activation marker) and Iba1 (global M/M $\Phi$  marker). The results showed that PSL-IL10 significantly suppressed the expression of GFAP (Fig. 6A and C) and decreased the numbers of CD68<sup>+</sup> M/M $\Phi$ s (Fig. 6B and D) in the peri-hematoma region at day 3 after ICH. Moreover, the levels of pro-inflammatory cytokine IL-1 $\beta$  and IL-6 in brain tissues were significantly lower in the PSL-IL10-treated mice than in other groups, as

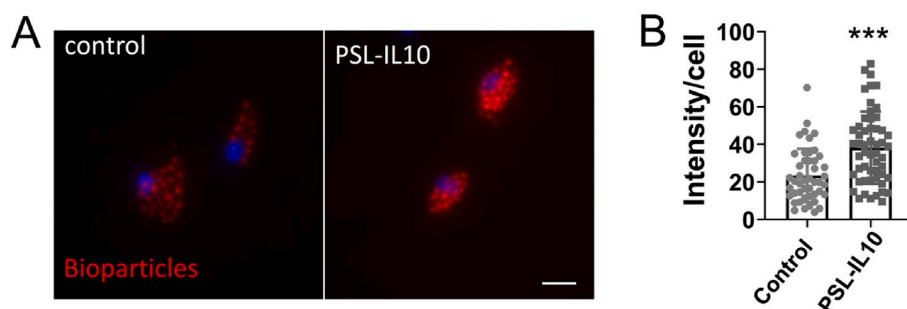


**Fig. 2.** PSL-IL10 enhances phagocytosis in cultured primary microglia. (A) Representative images showing the Bioparticles (Red) are phagocytosed by the cultured primary microglia. Microglia were incubated first with PSL-IL10 ( $3.2 \times 10^8$  particles/mL) for 24 h and then with pHrodo Zymosan Bioparticles for 3 h. Scale bar = 10  $\mu$ m. (B) Bar plot showing the fluorescent intensity of Bioparticles in cultured microglia were significantly higher in the PSL-IL10 treated microglia (Mann-Whitney *U* test, \*\*\*,  $p < 0.001$ ).

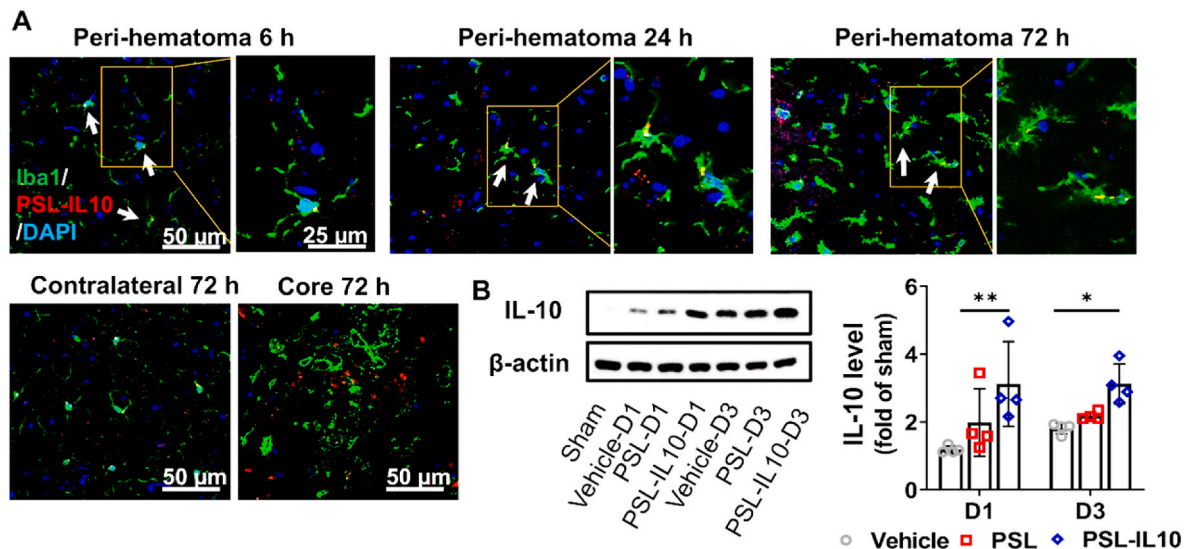


**Fig. 3.** Microglia/macrophages (M/MΦs) activation and PSL-IL10 distribution after ICH. PSL-IL10 labeled with rhodamine B was intranasally administered to ICH mice within 2 h after the administration of collagenase. **A**) The colocalization of M/MΦ (Iba1<sup>+</sup>, green) and PSL-IL10 (red) were observed under Leica SP8 confocal at 6, 24 and 72 h after ICH in brain regions of peri-hematoma, core hematoma and contralateral side. **B**) Western blotting of the IL-10 level at days 1 and 3 after ICH. The representative images are displayed, and the quantification results showed PSL-IL10 administration significantly elevated IL-10 levels both at day 1 and day 3 after ICH. n = 4 per group. Two-way ANOVA followed by Bonferroni post hoc was applied to detect the significant difference among the three groups. \*p < 0.05 and \*\*p < 0.01, data were expressed as mean ± SD. PSL: phosphatidylserine-containing liposomes. PSL-IL10: PSL-conjugated 0.3 μg IL-10.

revealed by ELISA (Fig. 6E). These results collectively demonstrated PSL-IL10 exerted strong immunomodulation effects, which are beneficial for the repair of ICH-induced injury.

### 3.6. PSL-IL10 enhanced M/MΦ phagocytosis function after ICH

We then investigated the effect of PSL-IL10 on M/MΦ morphology and phagocytosis function. The data are shown in Fig. 7A–F. To quantitatively assess the morphometric change of M/MΦ, we used the NeuroLucida software to analyze the Iba1<sup>+</sup> cells obtained on day 3 post-ICH. Many M/MΦs in all ICH groups exhibited larger cell soma size than sham microglia (Fig. 7B). Although no significant differences in total dendrite length (Fig. 7C) and node numbers (Fig. 7F) were observed, M/MΦs collected from PSL-IL10-treated mice exhibited significantly shorter average dendrite length (Fig. 7D) but an increase in the number of these short dendrites (Fig. 7E) compared with other groups.

To explore whether the differences in M/MΦ morphological characteristics were associated with M/MΦ function alteration, we isolated M/MΦs at day 1 post-ICH and cultured them in 6-well plates for 16 h to perform a phagocytosis assay. The cells had large soma without an abundant number of long processes (Fig. 7G). The M/MΦs collected from the PSL-IL10 treatment group were capable of engulfing many more beads as evidenced by the significantly increased red fluorescence intensity in these cells compared to cells from other groups (Fig. 7G). This result indicates that PSL-IL10 augments M/MΦ phagocytosis function after ICH. To further confirm the increased phagocytic capacity was associated with an altered cytokine phenotype [61], we also extracted mRNA from the collected M/MΦs and performed real-time PCR to measure the levels of pro-inflammatory (*IL-1β* and *IL-6*) and anti-inflammatory (*IL-4* and *Arg-1*) cytokine. The results showed PSL-IL10 significantly inhibited *IL-1β* and *IL-6* gene expression and tended to increase *IL-4* and *Arg-1* levels (Fig. 7H). Collectively, the data demonstrated that PSL-IL10 strongly enhanced the phagocytosis ability of M/MΦ and reduce the pro-inflammatory cytokine expression.

### 3.7. PSL-IL10 activated STAT3 signaling pathway and upregulated M/MΦ CD36 expression

We then conducted studies to investigate the contributions of the STAT3 signaling pathway to the M/MΦ modulating effects of PSL-IL10. Firstly, we detected the expression of total STAT3, STAT3 phosphorylation (pSTAT3), and CD36 by Western blot at day 1 and day 3 after ICH. Our results showed that PSL-IL10 significantly upregulated the expression level of CD36 (Fig. 8A and B) and pSTAT3 (Fig. 8A and C) on days 1 and 3. Notably, immunostaining results revealed that the higher CD36 were mainly expressed in M/MΦs (Iba1<sup>+</sup>) at day 3 after ICH in the PSL-IL10-treated group (Fig. 8D and E). Then, we used a conditional M/MΦ-targeted CD36 knockout mouse model (Lysm<sup>Cre</sup> ± CD36<sup>fllox/fllox</sup>, L-CD36) to confirm that the regulation effect of PSL-IL10 highly depends on CD36. As expected, in the L-CD36 mice, PSL-IL10 administration resulted in no significant improvement in ICH outcomes, neither the hematoma size on day 7 (Fig. 8F), nor the neurologic deficit score from day 1–7 (Fig. 8G). Thus, CD36 and related signaling pathways are central to the anti-inflammation effect of PSL-IL10.

## 4. Discussion

In this study, we developed a M/MΦs-targeted, nanoparticulate IL-10 therapy for effectively treating ICH. The key findings of our study are: 1) after intranasal administration, the developed nanoparticulate PSL-IL10 could accelerate hematoma resolution and improve ICH outcomes in a dose-dependent manner; 2) the efficacy of PSL-IL10 is attributed to its M/MΦs-targeting ability and regulation effects on M/MΦ; 3) the activation of STAT3 signaling pathway and upregulation of M/MΦ CD36 expression are likely the central mechanisms attributed to the effects of PSL-IL10. Our study demonstrated the promise and potential of PSL-IL10 as a new, effective therapy for treating ICH.

While administration of IL-10 has been widely tested as an immunomodulating intervention for various diseases, its clinical efficacy has yet to be established. Formidable challenges in applying IL-10 include the insufficient delivery efficiency to the disease sites [25] and complex pharmacological effects, such as reduced hemoglobin and thrombocyte counts and anemia, following systemic administration [27]. An

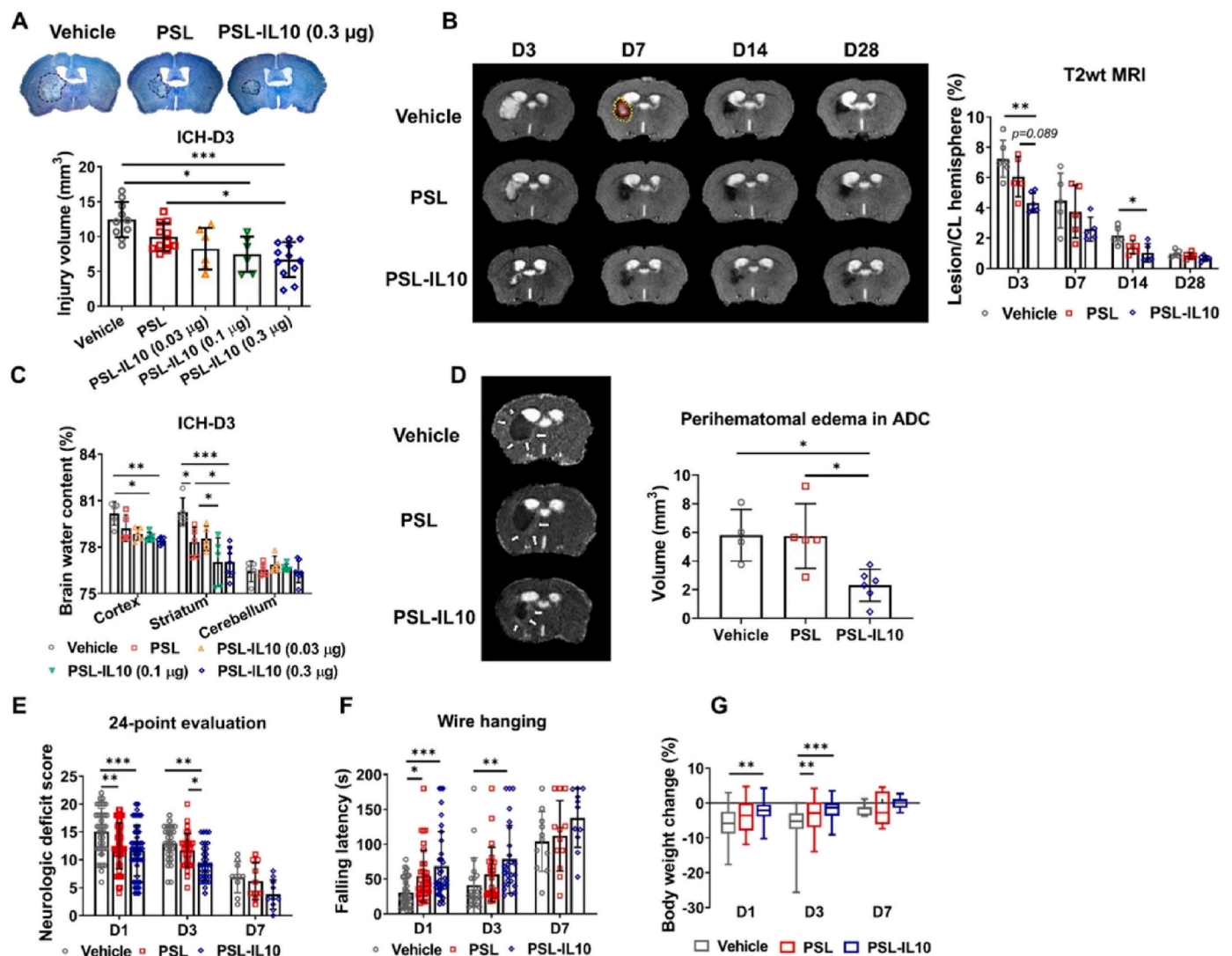


**Fig. 4.** Evaluation of the therapeutic effects of PSL-IL10 in ICH mice. **A)** Injury volume measured by Luxol fast blue/crystal violet staining. Top: representative staining images of mice that received saline, PSLs and PSL-IL10 (0.3 µg IL-10) intranasally. Bottom: Bar plots showing the calculated lesion volume at 3 days after ICH in different groups (n = 6–11). **B)** Injury volumes measured by T2-weighted (T2wt) MRI. Left: T2w images of three representative mice at 3, 7, 14 and 28 days after ICH. As an example, the hematoma region is outlined with a red line and the lesion area is outlined with a yellow dashed for the 7-day vehicle group image. Right: Ratio (%) of hemorrhagic lesion volume to the contralateral (CL) hemisphere volume in different groups (n = 5–6). **C)** Brain water content was measured at day 3 after ICH. n = 5–7 per group. **D)** Perihematomal edema measured using Diffusion MRI. Left: apparent diffusion coefficient (ADC) maps of three representative mice treated with saline, PSLs, and PSL-IL10, respectively. White arrows indicate the vasogenic edema regions that exhibit high ADC values. Right: Bar plots showing the mean edema volume in each group (n = 4–6). **E)** 24-point neurologic deficit score assessment on days 1, 3 and 7 after ICH (n = 10–47). **F)** Falling latency on days 1, 3 and 7 after ICH measured by wire hanging test (n = 10–47). **G)** Box-and-whisker plot of the change (%) in body weight on days 1, 3 and 7 after ICH with respect to that before ICH. n = 10–40 per group. Mixed-effects model or one-way ANOVA followed by Bonferroni post hoc was applied to detect a significant difference. \**p* < 0.05, \*\**p* < 0.01 and \*\*\**p* < 0.001, data were expressed as mean ± SD in panel A–F.

additional challenge for use in treating brain disorders is the poor penetration through the blood–brain barrier [62]. Thus, a more efficient method to deliver therapeutic IL-10 to M/MΦs in the brain after ICH is anticipated to dramatically improve its therapeutic efficacy.

Toward this goal, we chose to use PSL-IL10 to improve the selective delivery of IL-10 in ICH. While PSL-IL10 has been used to enhance the anti-inflammatory effect in obese mice [46], to the best of our knowledge, the present study is the first study that successfully employs PSL for M/MΦs-targeted delivery of IL-10 to treat neurologic disorders with significantly improved therapeutic outcomes. Such a design synergizes the M/MΦ-targeting ability of PSLs and the anti-inflammatory effects of IL-10 and PSLs [46]. In addition, we employed intranasal administration to further enhance the delivery efficiency because intranasal administration can be more effective for intracranial delivery than systemic administration routes [63]. As a result, our approach has shown

substantially higher IL-10 delivery in perihematomal regions and even in the hematoma core. Our observation is in line with other studies using phosphatidylserine as an “eat-me” signal to target M/MΦs [46,64]. Attributed to the delivery of a sufficient amount of exogenous IL-10 to the regions under ICH-induced injury, we observed immunomodulation effects on M/MΦs, reduced perihematomal edema, accelerated hematoma clearance, reduced neurologic deficit behavior scores, and less body weight loss, which is similar with the previously reported therapeutic effects of IL-10 against ICH [65,66]. Moreover, the improved outcomes after ICH were more consistent with PSL-IL10 than with PSLs or IL-10 alone, indicative of the effectiveness of combining IL-10 with PSLs. In a previous study by Xu et al., a liposomes formulation of IL-4 was shown to effectively promote hematoma resolution, reduce brain injury, and improve long-term functional recovery in mouse models of ICH [17]. This research also leveraged the intranasal administration of

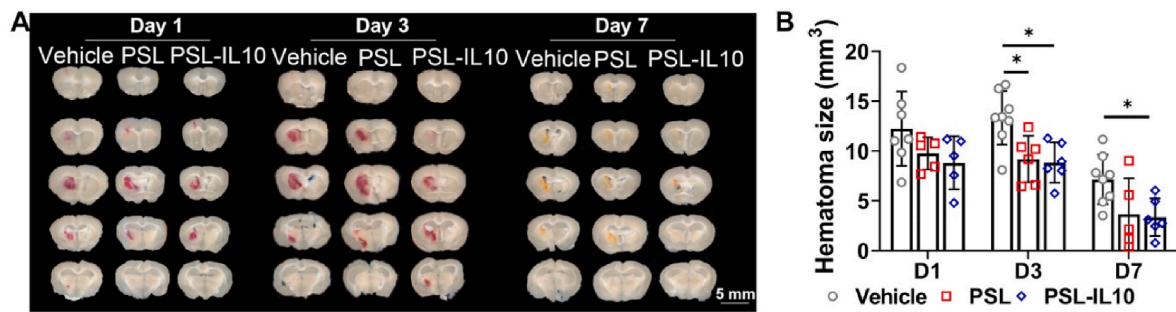


**Fig. 5.** PSL-IL10 promoted hematoma resolution after ICH. A) The representative pictures showed 1-mm depth serial fresh brain coronal slices from each group. B) Average hematoma size calculated from fresh brain sections in each group, which showed that PSL-IL10 significantly reduced hematoma size at days 3 and 7 after ICH. n = 5–8 per group.

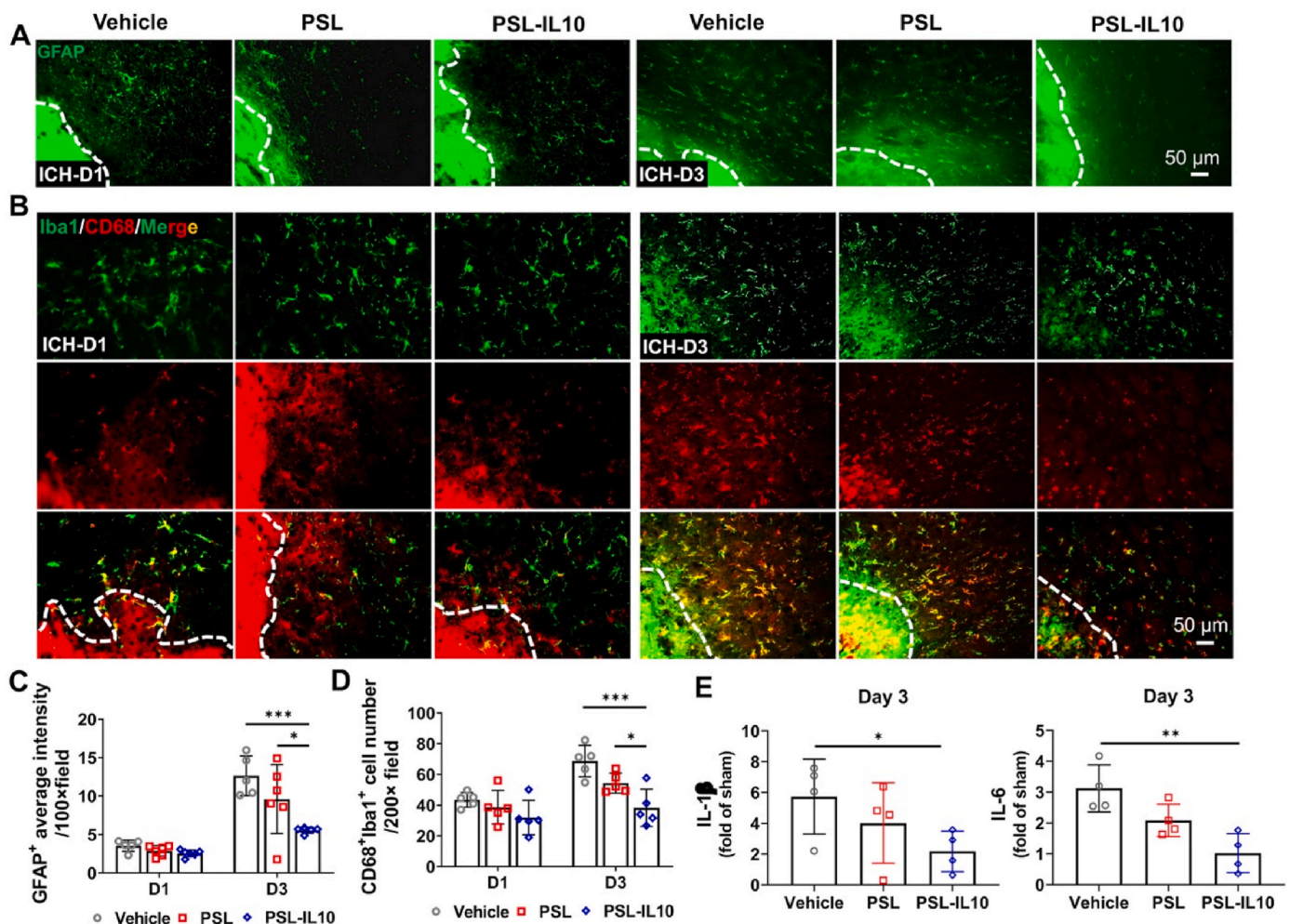


**Fig. 6.** PSL-IL10 inhibited glial activation and neuroinflammation on day 3 after ICH. A) Representative images of immunostaining of GFAP on days 1 and 3 post-ICH. B) Representative images of immunostaining of CD68 and Iba1 on days 1 and 3 post-ICH. C) Quantification of panel A. PSL-IL10 significantly declined GFAP<sup>+</sup> average intensity at day 3 after ICH relative to vehicle and PSL group. n = 5–6 per group. D) Quantification of Iba1 and CD68 double-positive cell numbers of panel B. PSL-IL10 significantly inhibited activated M/MΦs at day 3 after ICH relative to vehicle and PSL group. n = 5 per group. E) ELISA assay of proinflammatory cytokine IL-1β and IL-6 in brain tissue at 3 days after ICH. PSL-IL10 significantly decreased IL-1β and IL-6 levels. n = 4 per group. One-way, two-way ANOVA or mixed-effects model followed by Bonferroni post hoc was applied to detect a significant difference between multiple groups. \**p* < 0.05, \*\**p* < 0.01 and \*\*\**p* < 0.001, data were expressed as mean ± SD.

IL-4 in liposomal nanoparticulate form, underscoring the potential of nanoparticles and intranasal delivery in enhancing the efficiency of drug delivery in ICH, a finding that aligns with our study. A notable observation is that our PSL-IL10 demonstrates efficacy at a significantly lower dosage (0.3 μg IL-10 per mouse, or 12 μg/kg) in comparison to IL-4 (50

μg/kg body weight). This increased efficacy could be attributed to the use of PS-liposomes. Future comparative studies are warranted to systematically evaluate the relative efficacies of these two nanoparticulate drugs.

The intranasal administration route has drawn increased interest as a

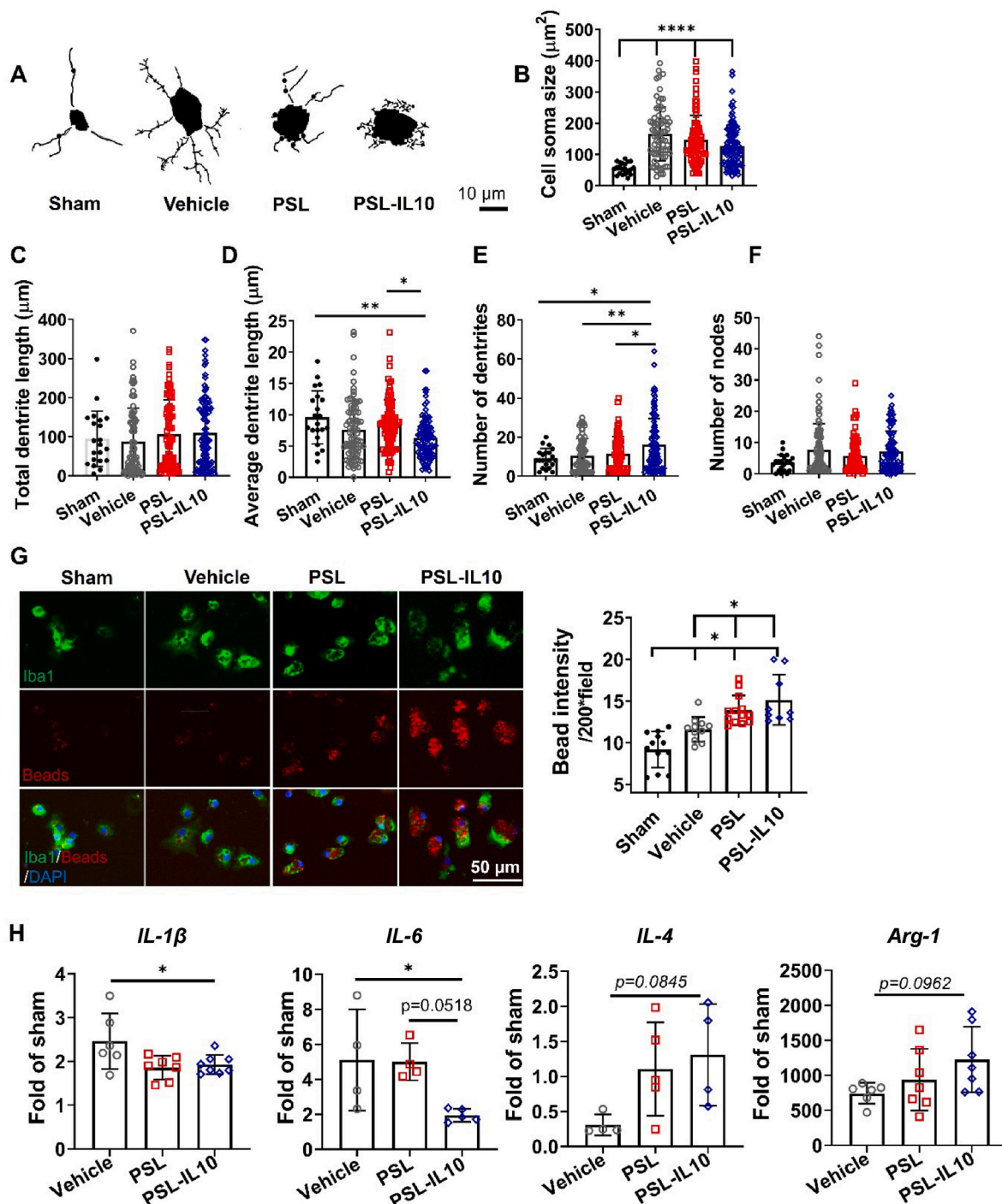


**Fig. 7.** PSL-IL10 altered microglia morphology and enhanced M/MΦ phagocytosis function after ICH. A-F. The morphology of Iba1<sup>+</sup> cells on day 3 post-ICH was analyzed by NeuroLucida software. A) Representative Iba1<sup>+</sup> cell morphology processed by NeuroLucida software in each group; B-F. Quantification of cell soma size (B), total dendrite length (C), average dendrite length (D), dendrite numbers (E) and node numbers (F) from panel A. One dot stands for one cell collected from 3 to 6 animals per group. G) M/MΦs were ex vivo cultured to evaluate their phagocytosis ability. The pH-sensitive pHrodo® Red Zymosan Bioparticles were incubated with sorted M/MΦs. M/MΦs isolated from PSL-IL10-treated animals engulfed more Bioparticles compared with other groups. One dot stands for average intensity/well collected from n = 3–5 animals/group. H) Real-time PCR of sorted M/MΦs at day 1 after ICH. PSL-IL10 significantly inhibited the *IL1β* and *IL6* gene expression, whereas *IL4* and *Arg1* levels showed marginal increases. One-way ANOVA followed by Bonferroni post hoc was applied to detect a significant difference. \**p* < 0.05, \*\**p* < 0.01 and \*\*\*\**p* < 0.0001, data were expressed as mean ± SD.

means to enhance the brain-targeting efficiency in stroke [67–69]. Rather than crossing the BBB from the blood circulation (unlike IV injected liposomes), intranasally injected liposomes cross the nasal epithelium via the transcellular pathway (e.g., axonal transport) or paracellular pathway (or the “nose - brain barrier” and are transported

along the olfactory and trigeminal nerves) [70]. The size of liposomes is typically larger than 100 nm. If injected intravenously, the majority of nanoparticles will be sequestered by reticuloendothelial system (RES), ending up in the liver and spleen [71,72]. This imposes a formidable challenge to deliver a sufficient amount of drug to the damaged area

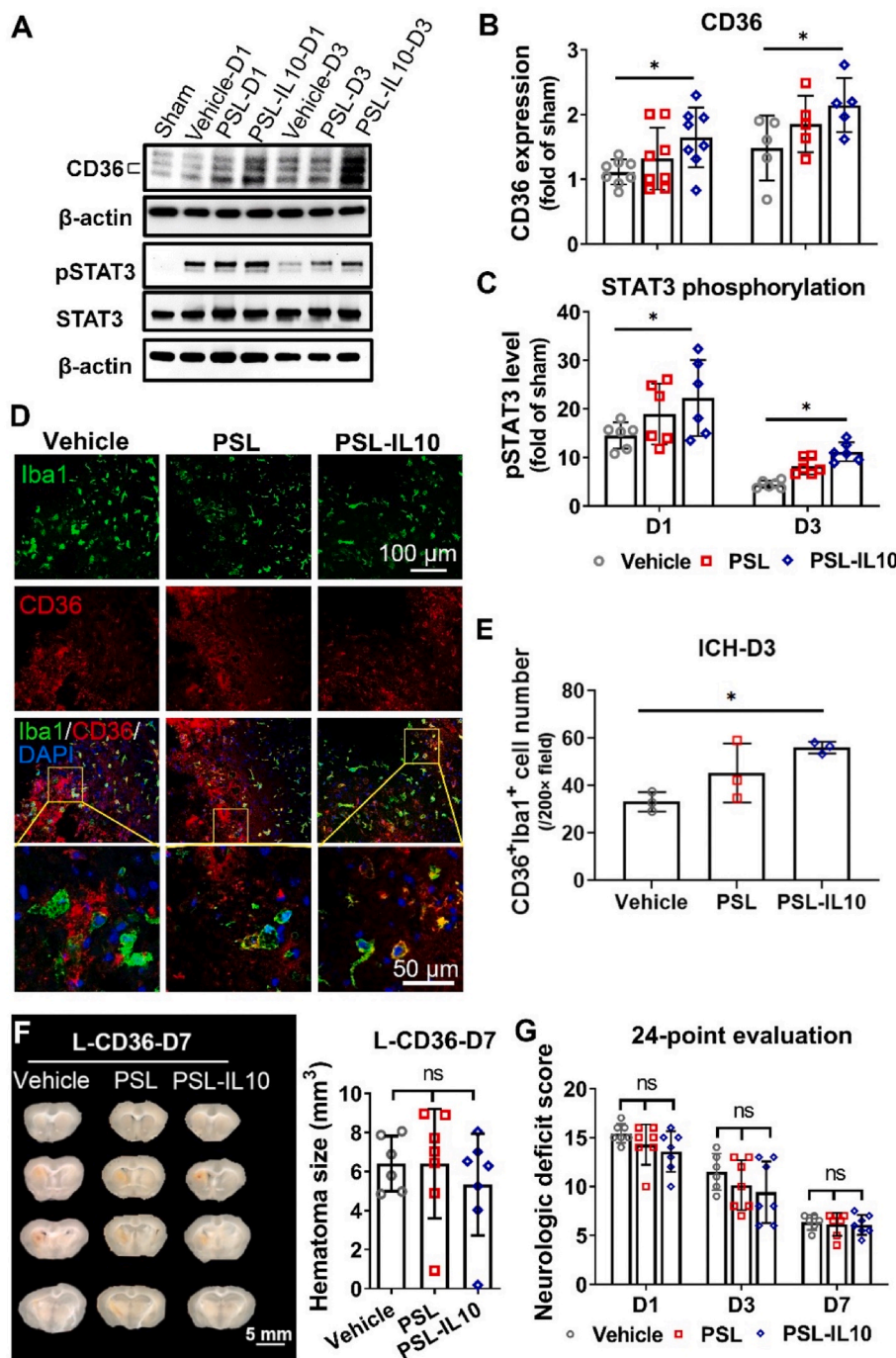


**Fig. 8. PSL-IL10 activated STAT3 signaling pathway and upregulated M/MΦ CD36 expression.** A. Western blot of CD36 expression, STAT3 phosphorylation (pSTAT3), and total STAT3 on days 1 and 3 after ICH. B–C. Quantification of CD36 (B) and pSTAT3 (C) from panel A showed PSL-IL10 significantly upregulated CD36 and pSTAT3 levels on days 1 and 3 after ICH. n = 5–9 per group. D. Representative immunostaining images of CD36 (red) and Iba1 (green) colocalization on day 3 after ICH. E. The quantification of panel D. The accumulation of CD36 was mainly expressed in M/MΦs in PSL-IL10-administered mouse brains. n = 3. F–G. Effects of PSL-IL10 on short-term outcomes of ICH-subjected M/MΦ-specific CD36 KO mice (*Lysm<sup>Cre</sup>CD36<sup>fllox/fllox</sup>, L-CD36*) mice. F. Hematoma size. PSL-IL10 administration did not alter the hematoma size on day 7. n = 6–7 per group. G. 24-point neurologic deficit score assessment. PSL-IL10 did not affect neurologic deficit score from day 1–7 on ICH-subjected L-CD36 mice. n = 6–7 per group. One-way ANOVA or mixed-effects model followed by Bonferroni post hoc was applied to detect a significant difference. \**p* < 0.05, data were expressed as mean ± SD. PSL: phosphatidylserine-containing liposomes. PSL-IL10: PSL-conjugated 0.3 μg IL10.

following ICH. Thus, intranasal delivery is a simpler and direct way for brain targeting, which minimizes exposure of peripheral organs to the drug and substantially reduces the likelihood of circulatory toxicity and adverse side effects. Additionally, drugs administered via intranasal delivery reach the CNS considerably faster, often within minutes, compared to peripheral administration. This rapidity can be a game-changer for drugs that degrade quickly and may otherwise be unsuitable. Finally, intranasal drug delivery is being investigated extensively in clinical trials for a wide array of therapies, including proteins, peptides, and stem cells. Currently, there are 141 open clinical trials recruiting patients to study intranasal delivery of therapies for various brain disorders. For example, promising results have been reported from a clinical trial in which intranasal delivered V2 vasopressin receptor agonist 1-desamino-8-D-arginine vasopressin (DDAVP)

improved speech function in 79% of cases in stroke patients [73].

Our study provided mechanistic evidence by which PSL-IL10 exerts its therapeutic effects via regulating the function of M/MΦs. In vitro data first showed that PSL-IL10 regulated M/MΦs to express less pro-inflammatory and more anti-inflammatory cytokines, indicative of anti-inflammatory polarization [61]. In vivo data also confirmed the effects of PSL-IL10 on inhibiting the presence of reactive astrocytes and CD68-positive reactive M/MΦs. Furthermore, we observed that the M/MΦs isolated from PSL-IL10-treated ICH mice have increased phagocytic capacity in bead uptake. Interestingly, PSL-IL10 treatment also altered the morphological appearance of microglia as characterized by more dendrite numbers with shorter average dendrite length than in the other ICH groups, although it is appreciated that morphology does not necessarily have one-to-one correspondence with function [74]. The

microglia that have taken up IL-10 will have already been exposed to the phosphatidylserine “eat me” signal, and the combination of this signal with IL-10 could have produced the distinct morphological appearance. Overall, these findings are in good agreement with other studies that reported a correlation between elevated M/M $\Phi$  phagocytosis capacity and accelerated hematoma resolution and improved ICH outcomes [17, 75,76].

To further illustrate the potential molecular mechanisms attributed to the therapeutic effects of PSL-IL10, we also investigated the contribution of the STAT3 signaling pathway in the PSL-IL10 treatment. The STAT3 signaling pathway is stimulated not only by the IL-10/IL-10 receptor interaction [25,77] but also by PS/PS receptor interaction [78, 79], which is another rationale for using PSL-IL10. Our data show a strongly elevated level of both STAT3 phosphorylation (pSTAT3) and CD36 on days 1 and 3 after ICH. When applied to CD36 knockout mouse model (LysM<sup>Cre</sup>  $\pm$  CD36<sup>flox/flox</sup>, L-CD36), PSL-IL10 exhibited no significant effects, thereby indicating that the function of PSL-IL10 highly depends on CD36. CD36 is a key phagocytosis effector for microglia, macrophages, and monocytes [80–82], and it has been reported to play a central role in promoting hematoma clearance both in ICH patients and animal models [18,82,83]. CD36 mediates the phagocytotic activity of M/M $\Phi$  [84] by binding to the PS of apoptotic cells [85]. Hence, the use of PSL as a platform to deliver IL-10 would take advantage of the PS-CD36 axis and result in more uptake of PSLs (and hence PSL-IL10) in IL-10-activated, CD36-overexpressed M/M $\Phi$ s, which serves as a gain-in-function to markedly increase the phagocytosis potency of M/M $\Phi$ s.

Our study has several limitations. First, although our study showed that CD36 is one of the essential molecular mechanisms for the protective effects of PSL-IL10 on the brain following ICH, other molecular mechanisms, for instance, CD47 [86] and CD163 [87], may also exist. Furthermore, PSL itself may stimulate other immune cells, such as CD8<sup>+</sup> T cells, through binding with TIM3 receptor on the CD8<sup>+</sup> T cells, leading to increased release of cytokine IL-13, which will promote M/M $\Phi$ s to produce more IL-10 [88]. Thus, more comprehensive mechanistic studies are warranted for a complete understanding of the contribution of each key molecule and signal pathway in the treatment of ICH. In the present study, we chose a liposome formulation containing 54% based on previous report to ensure a strong binding affinity Tim4, and hence endocytosis [50]. In fact, several studies have confirmed that PSL with 50% PS were effective for inducing M2-type polarization macrophages and exerting anti-inflammatory effects [89,90]. Nevertheless, further refinement of the liposome formulation is essential to optimize the delivery of IL-10 and boost the therapeutic effects on ICH. In this study, we administered PSL-IL10 at 2 h following ICH, a time point used in our previous treatment study [76]. This time point was chosen based on the temporal resolution of phenotypic change in CD11b-positive microglial cells post ICH [91–93]. However, future investigation may be needed sort out the optimal time window for PSL-IL10 administration. In addition, future investigations of the contributions of sex and age to the overall ICH outcomes in mice are needed to demonstrate the applicability of PSL-IL10 in different populations.

## 5. Conclusions

In this study, we developed a new approach for the targeted delivery of IL-10 to M/M $\Phi$  in the brain following ICH. Our study showed that PSL-IL10 could effectively ameliorate the outcomes of ICH, *i.e.*, accelerating hematoma resolution, reducing lesion sizes, and improving neurological functions. The anti-inflammatory effects of PSL-IL10 are exerted through the selective uptake in M/M $\Phi$  and consequentially regulating M/M $\Phi$  function and enhancing phagocytosis. The study showed the important mechanistic roles of STAT3 and CD36 in the M/M $\Phi$  modulating effect of PSL-IL10 on phagocytosis function. Collectively, our study demonstrated that PSL-IL10 is a promising M/M $\Phi$ -targeted therapy for ICH.

## Credit author statement

R Han, X Lan, X Han, RC Koehler, and G Liu designed the experiments and wrote the manuscript; Z Han, S Aafreen, W Wang, and G Liu prepared and characterized the drug delivery systems. R Han, X Han, and H Ren performed in vitro and animal experiments; T Zhu, X Hou, A Qian and R Han analyzed data; Z Han, G Liu, and X Lan performed MRI, and analyzed MRI data; all authors revised the manuscript.

## Declaration of competing interest

The authors declare that they have no known competing financial interests or personal relationships that could have appeared to influence the work reported in this paper.

## Data availability

Data will be made available on request.

## Acknowledgment

This research was supported by the National Institutes of Health R33HL161756 to GL, R01NS102583 to RCK, and the American Heart Association Career Development Award 19CDA34660065 to XL. We thank Dr. Xuhang Li from Johns Hopkins University for the gift of IL-10<sup>-/-</sup> mice; Dr. Ira J. Goldberg from New York University for the gift of CD36<sup>flox/flox</sup> mice and LysM<sup>Cre</sup>  $\pm$  CD36<sup>flox/flox</sup> mice; and Dr. George McNamara from Ross Fluorescence Imaging Center and ACCM Confocal Core at Johns Hopkins University for assistance with confocal microscopy.

## Appendix A. Supplementary data

Supplementary data to this article can be found online at <https://doi.org/10.1016/j.biomaterials.2023.122277>.

## References

- [1] V.L. Feigin, B.A. Stark, C.O. Johnson, G.A. Roth, C. Bisignano, G.G. Abady, et al., Global, regional, and national burden of stroke and its risk factors, 1990–2019: a systematic analysis for the Global Burden of Disease Study 2019, *Lancet Neurol.* 20 (2021) 795–820.
- [2] M. Schrag, H. Kirshner, Management of intracerebral hemorrhage: JACC focus seminar, *J. Am. Coll. Cardiol.* 75 (2020) 1819–1831.
- [3] M. Xue, V.W. Yong, Neuroinflammation in intracerebral haemorrhage: immunotherapies with potential for translation, *Lancet Neurol.* 19 (2020) 1023–1032.
- [4] R.F. Keep, Y. Hua, G. Xi, Intracerebral haemorrhage: mechanisms of injury and therapeutic targets, *Lancet Neurol.* 11 (2012) 720–731.
- [5] K. Lim-Hing, F. Rincon, Secondary hematoma expansion and perihemorrhagic edema after intracerebral hemorrhage: from bench work to practical aspects, *Front. Neurol.* 8 (2017) 74.
- [6] A. Shoamanesh, A.H. Katsanos, Combatting secondary injury from intracerebral hemorrhage with supplemental antioxidant therapy, *Stroke* 52 (2021) 1182–1184.
- [7] A.D. Mendelow, B.A. Gregson, H.M. Fernandes, G.D. Murray, G.M. Teasdale, D. T. Hope, et al., Early surgery versus initial conservative treatment in patients with spontaneous supratentorial intracerebral haematomas in the International Surgical Trial in Intracerebral Haemorrhage (STICH): a randomised trial, *Lancet* 365 (2005) 387–397.
- [8] A.D. Mendelow, B.A. Gregson, E.N. Rowan, G.D. Murray, A. Gholkar, P. M. Mitchell, et al., Early surgery versus initial conservative treatment in patients with spontaneous supratentorial lobar intracerebral haematomas (STICH II): a randomised trial, *Lancet* 382 (2013) 397–408.
- [9] A.L. de Oliveira Manoel, Surgery for spontaneous intracerebral hemorrhage, *Crit. Care* 24 (2020) 45.
- [10] D.F. Hanley, R.E. Thompson, M. Rosenblum, G. Yenokyan, K. Lane, N. McBee, et al., Efficacy and safety of minimally invasive surgery with thrombolysis in intracerebral haemorrhage evacuation (MISTIE III): a randomised, controlled, open-label, blinded endpoint phase 3 trial, *Lancet* 393 (2019) 1021–1032.
- [11] X. Lan, X. Han, Q. Li, Q.W. Yang, J. Wang, Modulators of microglial activation and polarization after intracerebral haemorrhage, *Nat. Rev. Neurol.* 13 (2017) 420–433.

- [12] R.A. Taylor, C.F. Chang, B.A. Goods, M.D. Hammond, B. Mac Grory, Y. Ai, et al., TGF-beta1 modulates microglial phenotype and promotes recovery after intracerebral hemorrhage, *J. Clin. Invest.* 127 (2017) 280–292.
- [13] C. Jiang, Y. Wang, Q. Hu, J. Shou, L. Zhu, N. Tian, et al., Immune changes in peripheral blood and hematoma of patients with intracerebral hemorrhage, *Faseb. J.* 34 (2020) 2774–2791.
- [14] H.Y. Yong, K.S. Rawji, S. Ghorbani, M. Xue, V.W. Yong, The benefits of neuroinflammation for the repair of the injured central nervous system, *Cell. Mol. Immunol.* 16 (2019) 540–546.
- [15] R. Dasari, F. Bonsack, S. Sukumari-Ramesh, Brain injury and repair after intracerebral hemorrhage: the role of microglia and brain-infiltrating macrophages, *Neurochem. Int.* 142 (2021), 104923.
- [16] H. Ren, R. Han, X. Chen, X. Liu, J. Wan, L. Wang, et al., Potential therapeutic targets for intracerebral hemorrhage-associated inflammation: an update, *J. Cerebr. Blood Flow Metabol.* 40 (2020) 1752–1768.
- [17] J. Xu, Z. Chen, F. Yu, H. Liu, C. Ma, D. Xie, et al., IL-4/STAT6 signaling facilitates innate hematoma resolution and neurological recovery after hemorrhagic stroke in mice, *Proc. Natl. Acad. Sci. U.S.A.* 117 (2020) 32679–32690.
- [18] Q. Li, X. Lan, X. Han, F. Durham, J. Wan, A. Weiland, et al., Microglia-derived interleukin-10 accelerates post-intracerebral hemorrhage hematoma clearance by regulating CD36, *Brain Behav. Immun.* 94 (2021) 437–457.
- [19] A. Liesz, A. Bauer, J.D. Hoheisel, R. Veltkamp, Intracerebral interleukin-10 injection modulates post-ischemic neuroinflammation: an experimental microarray study, *Neurosci. Lett.* 579 (2014) 18–23.
- [20] X. Xu, W. Gao, S. Cheng, D. Yin, F. Li, Y. Wu, et al., Anti-inflammatory and immunomodulatory mechanisms of atorvastatin in a murine model of traumatic brain injury, *J. Neuroinflammation* 14 (2017) 167.
- [21] P. Maiti, S. Peruzzaro, N. Kolli, M. Andrews, A. Al-Gharaibeh, J. Rossignol, et al., Transplantation of mesenchymal stem cells overexpressing interleukin-10 induces autophagy response and promotes neuroprotection in a rat model of TBI, *J. Cell Mol. Med.* 23 (2019) 5211–5224.
- [22] J.P. Barrett, R.J. Henry, S. Villapol, B.A. Stoica, A. Kumar, M.P. Burns, et al., NOX2 deficiency alters macrophage phenotype through an IL-10/STAT3 dependent mechanism: implications for traumatic brain injury, *J. Neuroinflammation* 14 (2017) 65.
- [23] L. Achmus, J. Ruhnau, S. Grothe, B. von Sarnowski, B.M. Broker, A. Dressel, et al., Stroke-induced modulation of myeloid-derived suppressor cells (MDSs) and IL-10-producing regulatory monocytes, *Front. Neurol.* 11 (2020), 577971.
- [24] P.J. Murray, The primary mechanism of the IL-10-regulated antiinflammatory response is to selectively inhibit transcription, *Proc. Natl. Acad. Sci. U.S.A.* 102 (2005) 8686–8691.
- [25] X. Wang, K. Wong, W. Ouyang, S. Rutz, Targeting IL-10 family cytokines for the treatment of human diseases, *Cold Spring Harbor Perspect. Biol.* 11 (2019).
- [26] J.F. Colombel, P. Rutgeerts, H. Malchow, M. Jacyna, O.H. Nielsen, J. Rask-Madsen, et al., Interleukin 10 (Tenovil) in the prevention of postoperative recurrence of Crohn's disease, *Gut* 49 (2001) 42–46.
- [27] F.E. Buruiana, I. Sola, P. Alonso-Coello, Recombinant human interleukin 10 for induction of remission in Crohn's disease, *Cochrane Database Syst. Rev.* 11 (2010) CD005109.
- [28] S. Sherman, C.L. Cheng, G. Costamagna, K.F. Binmoeller, A. Poespoeck, G.P. Aithal, et al., Efficacy of recombinant human interleukin-10 in prevention of post-endoscopic retrograde cholangiopancreatography pancreatitis in subjects with increased risk, *Pancreas* 38 (2009) 267–274.
- [29] A. Kumar, S. Zanotti, G. Bunnell, K. Habet, R. Anel, A. Neumann, et al., Interleukin-10 blunts the human inflammatory response to lipopolysaccharide without affecting the cardiovascular response, *Crit. Care Med.* 33 (2005) 331–340.
- [30] J. van Roon, S. Wijngaarden, F.P. Lafaber, C. Damen, J. van de Winkel, J. W. Bijlsma, Interleukin 10 treatment of patients with rheumatoid arthritis enhances Fc gamma receptor expression on monocytes and responsiveness to immune complex stimulation, *J. Rheumatol.* 30 (2003) 648–651.
- [31] E. Radwanski, A. Chakraborty, S. Van Wart, R.D. Huhn, D.L. Cutler, M.B. Affrime, et al., Pharmacokinetics and leukocyte responses of recombinant human interleukin-10, *Pharm. Res. (N. Y.)* 15 (1998) 1895–1901.
- [32] R.N. Fedorak, A. Gangl, C.O. Elson, P. Rutgeerts, S. Schreiber, G. Wild, et al., Recombinant human interleukin 10 in the treatment of patients with mild to moderately active Crohn's disease. The Interleukin 10 Inflammatory Bowel Disease Cooperative Study Group, *Gastroenterology* 119 (2000) 1473–1482.
- [33] A. Saxena, S. Khosraviyani, S. Noel, D. Mohan, T. Donner, A.R. Hamad, Interleukin-10 paradox: a potent immunoregulatory cytokine that has been difficult to harness for immunotherapy, *Cytokine* 74 (2015) 27–34.
- [34] I. Shlomovitz, M. Speir, M. Gerlic, Flipping the dogma - phosphatidylserine in non-apoptotic cell death, *Cell Commun. Signal.* 17 (2019) 139.
- [35] V.A. Fadok, D.L. Bratton, S.C. Frasch, M.L. Warner, P.M. Henson, The role of phosphatidylserine in recognition of apoptotic cells by phagocytes, *Cell Death Differ.* 5 (1998) 551–562.
- [36] A. Hochreiter-Hufford, K.S. Ravichandran, Clearing the dead: apoptotic cell sensing, recognition, engulfment, and digestion, *Cold Spring Harbor Perspect. Biol.* 5 (2013) a008748.
- [37] R. Sordi, A.C. Bet, A.M. Della Justina, G.C. Ramos, J. Assreuy, The apoptosis clearance signal phosphatidylserine inhibits leukocyte migration and promotes inflammation resolution in vivo, *Eur. J. Pharmacol.* 877 (2020), 173095.
- [38] Y. Narita, K. Shimizu, K. Ikemoto, R. Uchino, M. Kosugi, M.B. Maess, et al., Macrophage-targeted, enzyme-triggered fluorescence switch-on system for detection of embolism-vulnerable atherosclerotic plaques, *J. Contr. Release* 302 (2019) 105–115.
- [39] D.M. Cauvi, D. Hawisher, P.R. Dores-Silva, R.E. Lizardo, A. De Maio, Macrophage reprogramming by negatively charged membrane phospholipids controls infection, *Faseb. J.* 33 (2019) 2995–3009.
- [40] M.Z. Hosain, T. Mori, A. Kishimura, Y. Katayama, Synergy between phenotypic modulation and ROS neutralization in reduction of inflammatory response of hypoxic microglia by using phosphatidylserine and antioxidant containing liposomes, *J. Biomater. Sci. Polym. Ed.* 27 (2016) 290–302.
- [41] A. Partoazar, Z. Seyyedian, G. Zamanian, P.M. Saffari, A. Muhammadnejad, A. R. Dehpour, et al., Neuroprotective phosphatidylserine liposomes alleviate depressive-like behavior related to stroke through neuroinflammation attenuation in the mouse hippocampus, *Psychopharmacology (Berl)* 238 (2021) 1531.
- [42] P.M. Saffari, S. Alijanpour, N. Takzaree, M. Sahebgharani, S. Etemad-Moghadam, F. Noorbakhsh, et al., Metformin loaded phosphatidylserine nanoliposomes improve memory deficit and reduce neuroinflammation in streptozotocin-induced Alzheimer's disease model, *Life Sci.* 255 (2020), 117861.
- [43] G. Zamanian, A. Partoazar, S.M. Tavangar, A. Rashidian, P. Mirzaei, Q. Niaz, et al., Effect of phosphatidylserine on cirrhotic-induced hepatic encephalopathy: response to acute endotoxemia in cirrhotic rats, *Life Sci.* 253 (2020), 117606.
- [44] L. Huang, H. Tang, P. Sherchan, C. Lenahan, W. Boling, J. Tang, et al., The activation of phosphatidylserine/CD36/TGF-beta1 pathway prior to surgical brain injury attenuates neuroinflammation in rats, *Oxid. Med. Cell. Longev.* 2020 (2020), 4921562.
- [45] E.G. Pinto, L.R.S. Barbosa, R.A. Mortara, A.G. Tempone, Targeting intracellular Leishmania (L.) infantum with nitazoxanide entrapped into phosphatidylserine-nanoliposomes: an experimental study, *Chem. Biol. Interact.* 332 (2020), 109296.
- [46] R. Toita, T. Kawano, M. Murata, J.H. Kang, Anti-obesity and anti-inflammatory effects of macrophage-targeted interleukin-10-conjugated liposomes in obese mice, *Biomaterials* 110 (2016) 81–88.
- [47] Z. Chen, Y. Li, R. Airan, Z. Han, J. Xu, K.W.Y. Chan, et al., CT and CEST MRI bimodal imaging of the intratumoral distribution of iodinated liposomes, *Quant. Imag. Med. Surg.* 9 (2019) 1579–1591.
- [48] H. Liu, A. Jablonska, Y. Li, S. Cao, D. Liu, H. Chen, et al., Label-free CEST MRI detection of citicoline-liposome drug delivery in ischemic stroke, *Theranostics* 6 (2016) 1588–1600.
- [49] T. Harel-Adar, T. Ben Mordechai, Y. Amsalem, M.S. Feinberg, J. Leor, S. Cohen, Modulation of cardiac macrophages by phosphatidylserine-presenting liposomes improves infarct repair, *Proc. Natl. Acad. Sci. U.S.A.* 108 (2011) 1827–1832.
- [50] M. Hirose, T. Ueno, H. Nagumo, Y. Sato, K. Sakai-Kato, Enhancing the endocytosis of phosphatidylserine-containing liposomes through Tim4 by modulation of membrane fluidity, *Mol. Pharm.* 19 (2022) 91–99.
- [51] X. Lan, X. Han, Q. Li, J. Wang, (-)-Epicatechin, a natural flavonoid compound, protects astrocytes against hemoglobin toxicity via Nrf2 and AP-1 signaling pathways, *Mol. Neurobiol.* 54 (2017) 7898–7907.
- [52] P.A. Lapchak, J.H. Zhang, L.J. Noble-Haesuslein, RIGOR guidelines: escalating STAIR and STEPS for effective translational research, *Transl Stroke Res* 4 (2013) 279–285.
- [53] W.M. Clark, N.S. Lessov, M.P. Dixon, F. Eckenstein, Monofilament intraluminal middle cerebral artery occlusion in the mouse, *Neurol. Res.* 19 (1997) 641–648.
- [54] Q. Li, X. Han, X. Lan, Y. Gao, J. Wan, F. Durham, et al., Inhibition of neuronal ferroptosis protects hemorrhagic brain, *JCI Insight* 2 (2017), e90777.
- [55] J. Wang, A.D. Rogov, A.E. Tsirka, S.E. Tsirka, Protective role of tuftsin fragment 1-3 in an animal model of intracerebral hemorrhage, *Ann. Neurol.* 54 (2003) 655–664.
- [56] J. Yang, Q. Li, Z. Wang, C. Qi, X. Han, X. Lan, et al., Multimodality MRI assessment of grey and white matter injury and blood-brain barrier disruption after intracerebral haemorrhage in mice, *Sci. Rep.* 7 (2017), 40358.
- [57] X. Han, X. Zhao, X. Lan, Q. Li, Y. Gao, X. Liu, et al., 20-HETE synthesis inhibition promotes cerebral protection after intracerebral hemorrhage without inhibiting angiogenesis, *J. Cerebr. Blood Flow Metabol.* 39 (2019) 1531–1543.
- [58] X. Han, X. Lan, Q. Li, Y. Gao, W. Zhu, T. Cheng, et al., Inhibition of prostaglandin E2 receptor EP3 mitigates thrombin-induced brain injury, *J. Cerebr. Blood Flow Metabol.* 36 (2016) 1059–1074.
- [59] Q. Li, J. Wan, X. Lan, X. Han, Z. Wang, J. Wang, Neuroprotection of brain-permeable iron chelator VK-28 against intracerebral hemorrhage in mice, *J. Cerebr. Blood Flow Metabol.* 37 (2017) 3110–3123.
- [60] Q. Li, X. Lan, X. Han, J. Wang, Expression of tmem119/sall1 and ccr2/CD69 in FACS-sorted microglia- and monocyte/macrophage-enriched cell populations after intracerebral hemorrhage, *Front. Cell. Neurosci.* 12 (2018) 520.
- [61] S.A. Wolf, H.W. Boddeke, H. Kettenmann, Microglia in physiology and disease, *Annu. Rev. Physiol.* 79 (2017) 619–643.
- [62] A.J. Kastin, V. Akerstrom, W. Pan, Interleukin-10 as a CNS therapeutic: the obstacle of the blood-brain/blood-spinal cord barrier, *Brain Res Mol Brain Res* 114 (2003) 168–171.
- [63] F. Erdo, L.A. Bors, D. Farkas, A. Bajza, S. Gizurarson, Evaluation of intranasal delivery route of drug administration for brain targeting, *Brain Res. Bull.* 143 (2018) 155–170.
- [64] M.B. Naeini, V. Bianconi, M. Pirro, A. Sahebkar, The role of phosphatidylserine recognition receptors in multiple biological functions, *Cell. Mol. Biol. Lett.* 25 (2020) 23.
- [65] K. Zhou, Q. Zhong, Y.C. Wang, X.Y. Xiong, Z.Y. Meng, T. Zhao, et al., Regulatory T cells ameliorate intracerebral hemorrhage-induced inflammatory injury by modulating microglia/macrophage polarization through the IL-10/GSK3beta/PTEN axis, *J. Cerebr. Blood Flow Metabol.* 37 (2017) 967–979.
- [66] L.A. Sanni, W. Jarra, C. Li, J. Langhorne, Cerebral edema and cerebral hemorrhages in interleukin-10-deficient mice infected with *Plasmodium chabaudi*, *Infect. Immun.* 72 (2004) 3054–3058.

- [67] M.A. Javaid, M. Selim, S. Ortega-Gutierrez, S. Lattanzi, S. Zargar, D.A. Alaoui, et al., Potential application of intranasal insulin delivery for treatment of intracerebral hemorrhage: a review of the literature, *J. Stroke Cerebrovasc. Dis.* 31 (2022), 106489.
- [68] M. Guo, X. Ge, C. Wang, Z. Yin, Z. Jia, T. Hu, et al., Intranasal delivery of gene-edited microglial exosomes improves neurological outcomes after intracerebral hemorrhage by regulating neuroinflammation, *Brain Sci.* 13 (2023).
- [69] Y. Wang, M. Tian, J. Tan, X. Pei, C. Lu, Y. Xin, et al., Irisin ameliorates neuroinflammation and neuronal apoptosis through integrin  $\alpha$ v $\beta$ 5/AMPK signaling pathway after intracerebral hemorrhage in mice, *J. Neuroinflammation* 19 (2022) 82.
- [70] S.S. Hong, K.T. Oh, H.G. Choi, S.J. Lim, Liposomal formulations for nose-to-brain delivery: recent advances and future perspectives, *Pharmaceutics* 11 (2019).
- [71] W.C.W. Chan, Principles of nanoparticle delivery to solid tumors, *BME Frontiers* (2023) 4.
- [72] E. Blanco, H. Shen, M. Ferrari, Principles of nanoparticle design for overcoming biological barriers to drug delivery, *Nat. Biotechnol.* 33 (2015) 941–951.
- [73] S.G. Tsikunov, S.G. Belokoskova, Psychophysiological analysis of the influence of vasopressin on speech in patients with post-stroke aphasia, *Spanish J. Psychol.* 10 (2007) 178–188.
- [74] R.C. Paolicelli, A. Sierra, B. Stevens, M.E. Tremblay, A. Aguzzi, B. Ajami, et al., Microglia states and nomenclature: a field at its crossroads, *Neuron* 110 (2022) 3458–3483.
- [75] X. Zhao, G. Sun, S.M. Ting, S. Song, J. Zhang, N.J. Edwards, et al., Cleaning up after ICH: the role of Nrf2 in modulating microglia function and hematoma clearance, *J. Neurochem.* 133 (2015) 144–152.
- [76] C.F. Chang, J. Wan, Q. Li, S.C. Renfro, N.M. Heller, J. Wang, Alternative activation-skewed microglia/macrophages promote hematoma resolution in experimental intracerebral hemorrhage, *Neurobiol. Dis.* 103 (2017) 54–69.
- [77] L. Grant, K.D. Shearer, A. Czopek, E.K. Lees, C. Owen, A. Agouni, et al., Myeloid-cell protein tyrosine phosphatase-1B deficiency in mice protects against high-fat diet and lipopolysaccharide-induced inflammation, hyperinsulinemia, and endotoxemia through an IL-10 STAT3-dependent mechanism, *Diabetes* 63 (2014) 456–470.
- [78] J.H. van der Meer, T. van der Poll, C. van 't Veer, TAM receptors, Gas6, and protein S: roles in inflammation and hemostasis, *Blood* 123 (2014) 2460–2469.
- [79] M. Aziz, A. Jacob, A. Matsuda, P. Wang, Review: milk fat globule-EGF factor 8 expression, function and plausible signal transduction in resolving inflammation, *Apoptosis* 16 (2011) 1077–1086.
- [80] Y. Ren, R.L. Silverstein, J. Allen, J. Savill, CD36 gene transfer confers capacity for phagocytosis of cells undergoing apoptosis, *J. Exp. Med.* 181 (1995) 1857–1862.
- [81] I.S. Coraci, J. Husemann, J.W. Berman, C. Hulette, J.H. Dufour, G.K. Campanella, et al., CD36, a class B scavenger receptor, is expressed on microglia in Alzheimer's disease brains and can mediate production of reactive oxygen species in response to beta-amyloid fibrils, *Am. J. Pathol.* 160 (2002) 101–112.
- [82] H. Fang, J. Chen, S. Lin, P. Wang, Y. Wang, X. Xiong, et al., CD36-mediated hematoma absorption following intracerebral hemorrhage: negative regulation by TLR4 signaling, *J. Immunol.* 192 (2014) 5984–5992.
- [83] X. Zhao, G. Sun, J. Zhang, R. Strong, W. Song, N. Gonzales, et al., Hematoma resolution as a target for intracerebral hemorrhage treatment: role for peroxisome proliferator-activated receptor gamma in microglia/macrophages, *Ann. Neurol.* 61 (2007) 352–362.
- [84] E. Grajchen, E. Wouters, B. van de Haterd, M. Haidar, K. Hardonniere, T. Dierckx, et al., CD36-mediated uptake of myelin debris by macrophages and microglia reduces neuroinflammation, *J. Neuroinflammation* 17 (2020) 224.
- [85] V.A. Fadok, M.L. Warner, D.L. Bratton, P.M. Henson, CD36 is required for phagocytosis of apoptotic cells by human macrophages that use either a phosphatidylserine receptor or the vitronectin receptor (alpha v beta 3), *J. Immunol.* 161 (1998) 6250–6257.
- [86] W. Ni, S. Mao, G. Xi, R.F. Keep, Y. Hua, Role of erythrocyte CD47 in intracerebral hematoma clearance, *Stroke* 47 (2016) 505–511.
- [87] P. Philippidis, J.C. Mason, B.J. Evans, I. Nadra, K.M. Taylor, D.O. Haskard, et al., Hemoglobin scavenger receptor CD163 mediates interleukin-10 release and heme oxygenase-1 synthesis: antiinflammatory monocyte-macrophage responses in vitro, in resolving skin blisters in vivo, and after cardiopulmonary bypass surgery, *Circ. Res.* 94 (2004) 119–126.
- [88] S.K. Singh, K. Krukowski, G.O. Laumet, D. Weis, J.F. Alexander, C.J. Heijnen, et al., CD8+ T cell-derived IL-13 increases macrophage IL-10 to resolve neuropathic pain, *JCI Insight* 7 (2022).
- [89] L. Wu, Y. Kim, G.M. Seon, S.H. Choi, H.C. Park, G. Son, et al., Effects of RGD-grafted phosphatidylserine-containing liposomes on the polarization of macrophages and bone tissue regeneration, *Biomaterials* 279 (2021), 121239.
- [90] H. Quan, H.C. Park, Y. Kim, H.C. Yang, Modulation of the anti-inflammatory effects of phosphatidylserine-containing liposomes by PEGylation, *J. Biomed. Mater. Res.* 105 (2017) 1479–1486.
- [91] D.S. Shouval, A. Biswas, J.A. Goettel, K. McCann, E. Conaway, N.S. Redhu, et al., Interleukin-10 receptor signaling in innate immune cells regulates mucosal immune tolerance and anti-inflammatory macrophage function, *Immunity* 40 (2014) 706–719.
- [92] J. Wang, S. Dore, Heme oxygenase-1 exacerbates early brain injury after intracerebral haemorrhage, *Brain* 130 (2007) 1643–1652.
- [93] N. Weis, A. Weigert, A. von Knethen, B. Brune, Heme oxygenase-1 contributes to an alternative macrophage activation profile induced by apoptotic cell supernatants, *Mol. Biol. Cell* 20 (2009) 1280–1288.